



Validity of the Cauchy-Born rule applied to discrete cellular-scale models of biological tissues

by

**Y. Davit
J. M. Osborne
H. M. Byrne
D. Gavaghan
J. Pitt-Francis**

Validity of the Cauchy-Born rule applied to discrete cellular-scale models of biological tissues

Y. Davit

*Mathematical Institute, University of Oxford,
24-29 St Giles', Oxford, OX1 3LB, UK*

J. M. Osborne

*Department of Computer Science, University of Oxford,
Parks Road, Oxford OX1 3QD, UK*

H. M. Byrne

*Mathematical Institute, University of Oxford,
24-29 St Giles', Oxford, OX1 3LB, UK*

D. Gavaghan

*Department of Computer Science, University of Oxford,
Parks Road, Oxford OX1 3QD, UK*

J. Pitt-Francis

*Department of Computer Science, University of Oxford,
Parks Road, Oxford OX1 3QD, UK*

Abstract

The development of new models of biological tissues that consider cells in a discrete manner is becoming increasingly popular as an alternative to PDE-based continuum methods, although formal relationships between the discrete and continuum frameworks remain to be established. For crystal mechanics, the discrete-to-continuum bridge is often made by assuming that local atom displacements can be mapped homogeneously from the mesoscale deformation gradient, an assumption known as the Cauchy-Born rule (CBR). Although the CBR does not hold exactly for non-crystalline materials, it may still be used as a first order *approximation* for analytic calculations of effective stresses or strain energies. In this work, our goal is to investigate numerically the applicability of the CBR to 2-D cellular-scale models by assessing the mechanical behaviour of model biological tissues, including crystalline (honeycomb) and non-crystalline reference states. The numerical procedure consists in prescribing an affine deformation on the boundary cells and computing the position of internal cells. The position of internal cells is then compared with the prediction of the CBR and an average deviation is calculated in the strain domain. For centre-based models, we show that the CBR holds exactly when the deformation gradient is relatively small and the reference stress-free configuration is defined by a honeycomb lattice. We show further that the CBR may be used approximately when the reference state is perturbed from the honeycomb configuration. By contrast, for vertex-based models, a similar analysis reveals that the CBR does not provide a good representation of the tissue mechanics, even when the reference configuration is defined by a honeycomb lattice. The paper concludes with a discussion of the implications of these results for concurrent discrete/continuous modelling, adaptation of atom-to-continuum (AtC) techniques to biological tissues and model classification.

I. INTRODUCTION

Biological tissues are multiscale entities. Processes involved in their functioning occur over a broad spectrum of temporal and spatial scales. In tumour development, for example, genetic and epigenetic modifications disrupt cell homeostasis at the molecular-level (DNA damage and mutations), leading to anomalous behaviours at the cellular-level (apoptosis, abnormal proliferation) and tissue-level growth (morphogenesis, angiogenesis). Within communities of microorganisms attached to solid or liquid interfaces, micrometer-sized microbes can form intricate millimeter-sized structures (or smaller) interspersed with submillimeter fluid channels, termed biofilms. Furthermore, timescales may vary from milliseconds, for flow or signal transduction, to years, for significant tissue growth. Although there have been significant advances in our computational capabilities, simulating at the molecular scale over a period of several years is infeasible. In order to address these issues, a variety of theoretical approaches have been developed to model biological tissues (see discussions in Alarcón *et al.* [2], Osborne *et al.* [28]), leading to the emergence of two paradigms: discrete (cellular) and continuum (tissular) representations. *In the remainder of this work, we will focus on passive (i.e., without growth) tissue mechanics as described by these two paradigms.*

Within a cellular representation, all cells are modelled as discrete entities which can proliferate, migrate, die and interact with neighboring cells. This can be achieved in several different ways, including on-lattice descriptions for which cells and processes are represented on a fixed regular grid. Examples of on-lattice representations are cellular automata (see Moreira & Deutsch [24]) and cellular Potts models (also known as Graner-Glazier models, cf. Graner & Glazier [18]). By contrast, off-lattice models represent each cell by a set of points in space, independently of any grid. Examples of off-lattice models include centre-based models where cells are represented by a single point (e.g., sphere-based models in Drasdo & Höhme [10] or tessellation-based models in Meineke *et al.* [22]), and vertex-based models (see in Nagai & Honda [27]) where cells are represented by their vertices. With the continuum representation, the tissue is modelled via a system of partial differential equations (PDEs). The PDEs can also be discretized to allow for numerical solution but, in contrast with cellular-scale models, a typical mesh size will be much coarser than the characteristic length of a cell. Tissues are, therefore, described in an averaged sense, with properties evaluated between the cellular- and tissular-scales. Within this framework, tissue mechanics typically

rely on linear/nonlinear elastic or viscoelastic theories and cellular growth is introduced through constitutive evolution laws for macroscale parameters. One such method is based on a multiplicative decomposition of the deformation gradient, $\mathbf{F} = \mathbf{F}_p \cdot \mathbf{F}_a$, where \mathbf{F}_a represents the imposed (active) growth and \mathbf{F}_p is the (passive) mechanical response. Another approach relies upon an additive decomposition the Piola-Kirchhoff stress tensor (see Ambrosi & Pezzuto [4] for a detailed discussion of these models).

The two classes of models introduced above have their respective strengths and weaknesses. Cellular-scale descriptions can incorporate a substantial amount of information which may be particularly relevant to medical and biological applications. In tumour development, for instance, initial mutations occur within individual cells, a phenomenon that can only be adequately understood using cellular-scale models. Obviously, the disadvantage of such resolution is the computational expense, which exceeds current capabilities when dealing with large numbers of cells, for example when considering entire organs or even organisms (e.g., $\approx 10^{14}$ cells in the human body). Further, these models are often based on mathematical abstractions that can be difficult to relate to biophysically measurable properties of the problem of interest. Continuum-based approaches, on the other hand, are less computationally intensive and provide a more intuitive framework in which parameters and operators can be adjusted to fit experimental observations. However, they describe only an average behaviour of the tissue and have domains of validity which can be difficult to determine.

Although continuum and cellular-scale approaches have traditionally been used separately, there is evidence that they could be used in a complementary manner. Recent works have proposed such multiscale methods that aim to overcome issues with computational limitations without sacrificing precision. Hybrid concurrent discrete/continuous models, for instance, may be used for such purposes. Hybrid frameworks rely on the idea that, in many cases, a cellular-scale description is needed only in a limited region of the tissue where processes vary over short spatial or temporal scales. In the rest of the tissue, where characteristic times and lengths are significantly larger, continuum descriptions may be used. Kim *et al.* [21], Stolarska *et al.* [35] applied this idea to tumour spheroids, using a continuum approach to model the necrotic and quiescent zones and a discrete cellular-scale model within the relatively small and active peripheral region. From a practical point of view, such models are extremely appealing because they resolve many of the issues found when each approach is used individually: the computational cost of pure cellular-scale models and the

failure of continuum models to capture phenomena occurring on short scales. From a more fundamental perspective, however, there are a number of issues that require attention before this approach can be more widely used to develop models of biological tissues. Typical unresolved questions are: What boundary conditions should be imposed on the interface between discrete and continuum regions? Where should the interface be positioned? How should it evolve over time?

Interestingly, similar problems have emerged in atom-to-continuum (AtC) modelling where various multiscale strategies have been developed to deal with large deformations and dislocations in crystalline systems. Such multiscale methods include quasicontinuum (QC) [33], bridging scale [36], hybrid discrete/continuum with blending [12] or nonlocal techniques [32]. Blending techniques, for example, are used to treat boundaries in hybrid discrete/continuum formulations. Continuity conditions are imposed at the interface between the two distinct regions by defining an overlapping volume that is used to blend model variables, e.g. energy functionals, forces, stresses or displacements (see Badia *et al.* [5]). Another category of models, termed QC methods (see [23] for a thorough review of QC methods), aims to approximately solve the atomic-scale problem. The technique uses adaptive meshing and interpolation procedures inherited from finite element methods, in conjunction with physical approximations that allow for the reduction of the number of degrees of freedom of the problem (localization, CBR, strain/stress criteria, representative atoms). Peridynamic models are spatial nonlocal formulations that describe material mechanics by using an integro-differential formulation of momentum transport, an approach that avoids issues associated with cumbersome boundary conditions of concurrent models. *For all of these models, however, a means of bridging discrete and continuum scales is needed in order to develop clear relationships between both paradigms.* With hybrid modelling, for instance, the model used in the continuum region should correspond, in some sense, to the continuum limit of the discrete model and boundaries should be treated accordingly.

For cellular-scale models, this discrete-to-continuum (DtC) connection has been most widely studied in one spatial dimension (1-D), and is not yet available in higher-dimensional configurations. For example, Murray *et al.* [26] derived a continuum expression corresponding to a 1-D chain of overdamped cells. In this approach, the limit of discrete sums is considered to obtain differential operators that can be combined into a single nonlinear diffusion equation for cellular-density. Bodnar & Velasquez [6] studied the mathematical

behaviour of an integro-differential (nonlocal) equation for the cellular-density that can be interpreted as the continuum limit of a 1-D tissue model of overdamped particle interacting via conservative forces. Fozard *et al.* [13] used asymptotics to derive Darcy-like equations for momentum transport at the continuum scale. These approaches pave the way for future developments and provide insights into the large scale dynamics of cellular-scale models. However, their extension to higher-dimensional systems is not systematic. Such 2- or 3-D extensions are important because they provide a solid basis for: (1) relating the effective tissue-scale parameters to cellular-scale properties; (2) understanding the approximations associated with continuum models and establishing when continuum approaches are appropriate; (3) developing appropriate boundary conditions for hybrid concurrent models or adapting other AtC strategies to the biological context; and (4) creating classification methods for cellular-scale models via their continuum limit.

For crystal mechanics, this bridge can be obtained using the Cauchy-Born rule (CBR). The CBR is an assumption that can be used to pass information through scales by linearly relating the local microscale displacement field to the mesoscale deformation gradient. In this study, our goal is to analyse numerically the validity of the CBR for cellular-scale models of biological tissues with honeycomb and disordered reference states. *We will focus solely on passive tissue mechanics, i.e., we will not consider cellular growth.* To this end, we will use an approach similar to that of Aghaei *et al.* [1] and Friesecke & Theil [14]. We will consider a representative region of the tissue, impose an affine deformation on boundary nodes and calculate an average deviation from the CBR in the central region.

The remainder of this work is organized as follows. In Section II, we discuss in more detail the CBR and ideas underlying its application to cellular-scale models of biological tissues. In Section III, we present the modelling framework and the implementation of these models. In Section IV, we present results and their interpretation. Finally, in Section V, we discuss the implications of these results for discrete-to-continuum approaches, hybrid discrete/continuous modelling and model classifications.

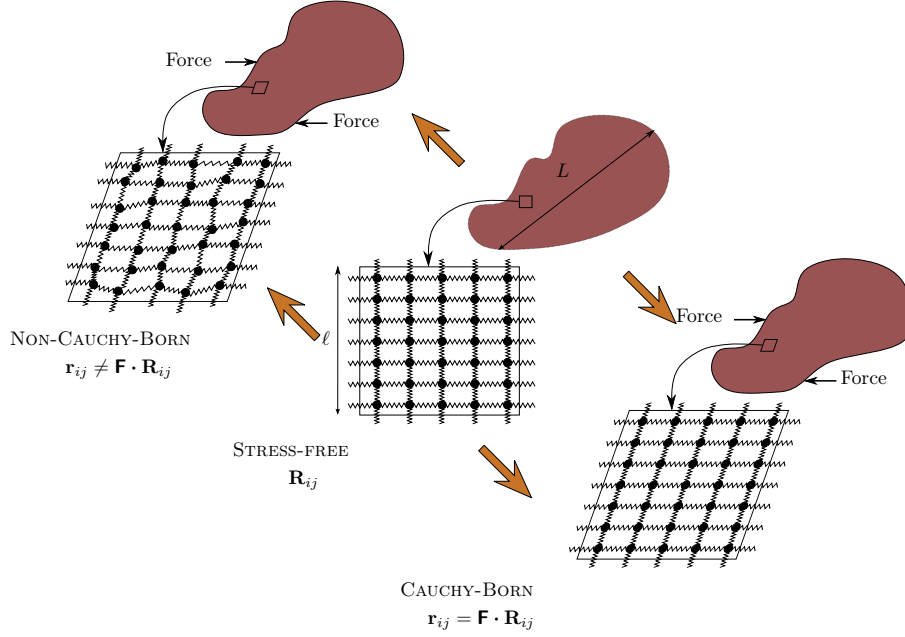


Figure 1. (Color online) Schematic representation of the CBR. The central picture shows the node positions in the reference (lattice) configuration. In the two other figures, forces applied at a macroscopic level induce deformation of the material. The bottom right configuration corresponds to displacements that satisfy the CBR, while the top left configuration describes displacements that do not, i.e., nodes are rearranging on an atomic lengthscale.

II. THE CAUCHY-BORN RULE

A. Definitions

The CBR was used by Cauchy [34] and Born [7] to derive expressions for the elastic modulus of a crystalline solid in terms of atomic-scale parameters. The rule is illustrated in Fig 1 and arises from the following considerations (see detailed discussion in [11]). First, consider a homogeneous crystalline material, characterised by the macroscopic lengthscale L ; and a unit cell for the crystal structure, characterised by the microscopic lengthscale ℓ . Suppose that a macroscopic stress/strain with a characteristic time, τ_M , initiates a deformation of this material and that relaxation at the microscopic scale is characterised by the time τ_μ . Now, impose the separation of lengthscales, $L \gg \ell$, so that each unit cell can be treated as a macroscopic point and the deformation gradient, \mathbf{F} , can be considered to be constant over each unit cell. Finally, assume that there is a separation of timescales,

$\tau_M \gg \tau_\mu$, so that the relaxation processes within each unit cell can be considered quasi-steady. The CBR states that all atoms within each unit cell will be displaced homogeneously. In other words, if \mathbf{r}_i (\mathbf{r}_j) is the quasi-steady position of atom i (j , respectively) in the stressed state and \mathbf{R}_i (\mathbf{R}_j) is the position of atom i (j , respectively) in the reference configuration, then

$$\mathbf{r}_{ij} \equiv \mathbf{r}_i - \mathbf{r}_j = \mathbf{F} \cdot (\mathbf{R}_i - \mathbf{R}_j) = \mathbf{F} \cdot \mathbf{R}_{ij}. \quad (1)$$

In conjunction with this relationship, a variety of methods can be used to derive the macroscale continuum equations. For example, methods based on discrete expressions of the Cauchy stress tensor [37] or strain density energies may be used.

B. Non-crystalline reference state

The CBR does not generally apply to non-crystalline materials because deformations occur inhomogeneously, i.e., stresses generate reorganization and relaxation of the (quenched) reference state on small lengthscales. However, it can be used to *approximate* amorphous solid continuum mechanics (see [3]), even though the calculation of effective properties may require the expression of the residual stresses in the reference state. In this work, the rationale for applying the CBR to cellular-scale models of biological tissues is threefold:

1. As discussed in [3], the validity of the CBR at the microscale translates the intuitive notion of solid behaviour at the macroscale: displacements about a stable equilibrium are locally homogeneous and do not generate node permutations, as is the case for fluids. In this sense, studying the validity of the CBR is similar to studying elastic continuum properties of biological tissues.
2. We will focus on structured reference states for which the CBR may be used as a first-order approximation to calculate homogenized continuum stresses and energies. Example tissues that exhibit spatially structured patterns include plants, wood, leaves, bones, ocular tissues, sponges or epithelia (see e.g. [17]). Two of the most common patterns are foam-like and honeycomb structures. Furthermore, the honeycomb reference state has often been used for modelling purposes. Therefore, honeycomb results can be used to study model mechanical behaviour in the continuum limit, for example to provide a means of comparison between cellular-scale models.

3. Tissue mechanics and morphogenesis are governed by a complex dynamical interplay between, among others, extracellular substances, fluids, cell membranes, cell cytoskeleta and intercellular protein junctions (see [19]). In these systems, large networks of biopolymers generate intercellular interactions that strengthen the elastic behaviour of the tissue as a whole. In particular, fibre networks are known to behave in a self-similar (affine) manner in some regions of parameter space (see [8] and [16]).

III. MODELLING FRAMEWORK

A. Cellular-scale models and Chaste

The computations presented in this paper were performed using Chaste (Cancer, heart and soft-tissue environment), an open-source modelling framework developed in C++ by the Department of Computer Science at the University of Oxford. Chaste includes a set of libraries and test suites for cellular-scale models of biological tissues with on-lattice and off-lattice descriptions. Chaste also handles cellular growth and provides various generic solvers for differential equations and boundary value problems that can be used for coupling cellular-scale models with systems of ODEs and PDEs. Further information about the code can be found in Pitt-Francis *et al.* [30] and on the website <http://www.cs.ox.ac.uk/chaste/>.

In this work, we will use Chaste’s 2-D off-lattice cellular-scale models, in particular we use two classes of models that we characterise as follows. Centre-based models (see Pathmanathan *et al.* [29]) simulate cell movement by concentrating mass at its centre, hence reducing computations to tracking a finite number of nodes (cell centres). Vertex-based models (see Honda *et al.* [20], Nagai & Honda [27]) view cells as polygons which can be characterised by the positions of their vertices. When considering centre-based models, we will distinguish between sphere- and tessellation-based models which differ in the way in which connectivity is determined, i.e., how neighbours are defined. For sphere-based models, connectivity is resolved via a radius of interaction see Fig 2a. For tessellation-based models, connectivity is resolved using a Voronoi tessellation and the corresponding Delaunay triangulation see Fig 2b. For vertex-based models connectivity is defined by a network of connected polygons see Fig 2c. When considering vertex-based models we will only consider cases for which connectivity is determined by the initial configuration.

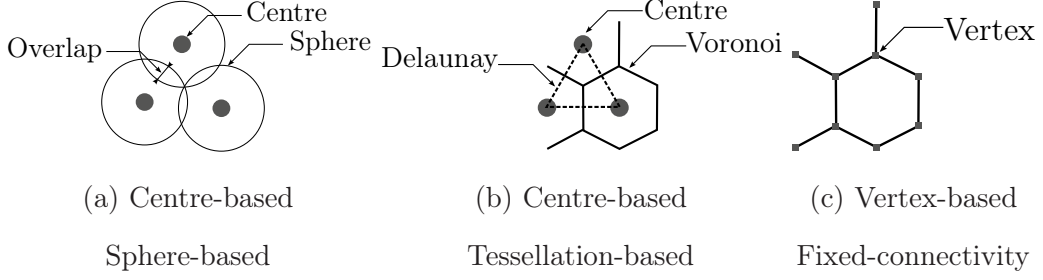


Figure 2. Schematics of the different modelling frameworks.

For each model, we assume that cell movement is overdamped, so that applying Newton’s law of motion to each node, i , supplies

$$\eta_i \frac{d\mathbf{r}_i}{dt} = \mathbf{f}_i, \quad (2)$$

where η_i is a damping coefficient/viscous drag that we fix to $(1.0 \text{ nN} \cdot h \cdot \mu\text{m}^{-1})$ for each node, i.e., approximately ten times larger than in Galle *et al.* [15]; \mathbf{r}_i is the position of node i (μm); t is the time variable in hours (h); and \mathbf{f}_i is the force on node i in nano-Newton (nN). We discretise Eq (2) using a forward Euler method so that the position of node i at time $t + \Delta t$ is determined from its position at time t via:

$$\mathbf{r}_i^{t+\Delta t} = \mathbf{r}_i^t + \frac{\Delta t}{\eta} \mathbf{f}_i. \quad (3)$$

Stability of the explicit discretization method requires that the timestep is carefully chosen. Here, we used $\Delta t = \frac{1}{120} h = 30 \text{ s}$ for centre-based models and $\Delta t = 1.8 \text{ s}$ for vertex-based models.

To complete our characterization of these cellular-scale models, we must define constitutive laws for the forces, \mathbf{f}_i . For centre-based models, we express these forces in terms of the nondimensionalized “overlap” parameter,

$$\delta = \frac{1}{\ell} (\|\mathbf{r}_{ij}\| - \ell_{ij}), \quad (4)$$

where $\ell_{ij} > 0$ is the rest length of the spring that connects nodes i and j ; and ℓ is a characteristic lengthscale (which we fix to $10 \mu\text{m}$). δ can be interpreted as a measure of the deviation from the rest length with a sign that determines the nature (attractive or repulsive) of the force. Unless stated otherwise, we assume that rest lengths are identical for all cells within the population and equal to ℓ . This may be written as $\ell_{ij} = \ell$ for any pair i, j . For centre-based models, we will use a cut-off length $\ell_c = 1.1 \times \ell$ which enforces a finite

	Type	Connectivity	Force
Model 1	Centre-based	Tessellation-based	Spring, \mathbf{f}_i^S
Model 2	Centre-based	Sphere-based	Quasi-spring, \mathbf{f}_i^{QS}
Model 3	Centre-based	Sphere-based	Nonlinear, \mathbf{f}_i^{NL}
Model 4	Vertex-based	Fixed	Nagai-Honda, \mathbf{f}_i^{NH}

Table I. Table summarizing the four models used in this paper. Each model is completely defined by a type (cellular- or vertex-based), a notion of connectivity (sphere-based, tessellation-based or initially fixed) and a force (S, QS, NL or NH).

distance of interaction between cells. In the remainder of this paper, we consider spring (S), quasi-spring (QS), and nonlinear (NL) forces for centre-based models and a Nagai-Honda (NH) force for the vertex based model. Details of all forces are given in the Appendix and models are summarized in Table I. For clarity, from here on, we will refer to each model by the number assigned in this table.

B. CBR tests

For AtC problems, the validity of the CBR has been studied in various systems. For example, Friesecke & Theil [14] studied analytically the behaviour of a network of atoms, initially positioned on a 2-D square lattice and interacting via harmonic springs. By prescribing an affine deformation on boundary nodes of a unit cell and studying the response of central nodes, they showed that particle locations predicted by the CBR are a minimizer of the net energy only in a limited region of parameter space. In particular, the validity of the CBR is restricted to relatively small deformation gradients. Aghaei *et al.* [1] studied the validity of the CBR numerically on a lattice of atoms interacting via the Sutton-Chen many-body potential. They also imposed a deformation on boundary atoms and observed the response of central atoms. By examining deviations from the CBR in the strain and stress domains, they could determine domains of validity. In this paper, we will follow a similar strategy and apply it to the cellular-scale models discussed above. In Fig 3, we illustrate how we distinguish between boundary and central nodes for a tessellation-based

model.

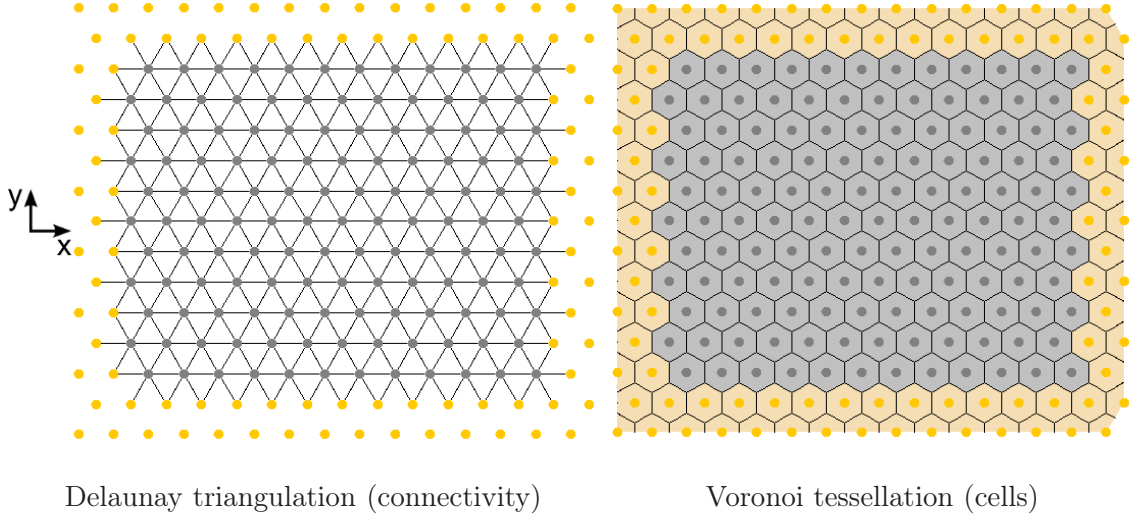


Figure 3. (Color online) Example population of centre-based tessellation-based cells. The Delaunay triangulation is plotted on the left-hand side and the corresponding Voronoi tessellation is plotted on the right-hand side. Boundary cells to which displacements are applied are colored in yellow. Central cells that are used to study deviations from the CBR are colored in grey.

Herein, positions are resolved within a Cartesian coordinate system that has its origin at the centre of mass of the cell population. x - and y -axis are oriented along natural horizontal and vertical directions, see Fig 3. Boundary nodes are displaced from positions \mathbf{R}_i in the reference state to \mathbf{r}_i by introducing a mesoscale deformation gradient \mathbf{F} so that

$$\mathbf{r}_i = \mathbf{F} \cdot \mathbf{R}_i. \quad (5)$$

Further, tension/compression and shear deformations are applied by using the following two tensors, $\mathbf{F}^{\text{T,C}}$ and \mathbf{F}^{S} :

$$\mathbf{F}^{\text{T,C}} \equiv \begin{bmatrix} 1 & 0 \\ 0 & \alpha_{\text{T,C}} \end{bmatrix}, \quad (6)$$

and

$$\mathbf{F}^{\text{S}} \equiv \begin{bmatrix} 1 & \alpha_{\text{S}} \\ 0 & 1 \end{bmatrix}. \quad (7)$$

Here, the deformation constant, α , fixes the amplitude of the deformation. We remark that with these notations, the reference configuration is given by $\alpha_{\text{T,C}} = 1$ for tension/compression and $\alpha_{\text{S}} = 0$ for shear.

For a given target value of α , boundary nodes were displaced by small increments ($\Delta\alpha = 2 \times 10^{-3}$) for centre-based models and ($\Delta\alpha = 1 \times 10^{-3}$) for vertex-based models. For centre-based models, the system was assumed to be at steady-state when either the average velocity over all nodes reached the critical value $10^{-7} \mu m \cdot h^{-1}$ or the total time for relaxation of this α -increment reached 10 hours. For vertex-based models, the system was assumed to be at steady-state when either the average velocity over all nodes reached the critical value $10^{-10} \mu m \cdot h^{-1}$ or the total time for relaxation of this α -increment reached 10 hours. Although results are not presented here, tests for convergence were performed by using fractions of these different steps. In some cases, presented below, we also imposed small perturbations, i.e., random motion of the cells, to further explore the stability of our results. This method was implemented by selecting, for each time-step, a random angle and enforcing a small jump of the node at this angle with a velocity of $10^{-1} \mu m \cdot h^{-1}$, i.e., an amplitude of $\approx 8.3 \cdot 10^{-4} \mu m$ for a timestep, $\Delta t = 1/120 h$. For simplicity, we refer to such random displacements as “Brownian”, although they are not meant to describe Brownian motion, but to address the sensitivity of our results to small perturbations.

The validity of the CBR was evaluated by comparing, in the strain domain, the computed positions of the central nodes with the predictions of the CBR (see Eq (1)). Deviation was measured via the following expression

$$\text{deviation} \equiv \frac{1}{N} \sum_{i=1}^N \|\mathbf{r}_i - \mathbf{r}_i^{CBR}\| = \frac{1}{N} \sum_{i=1}^N \|\mathbf{r}_i - \mathbf{F} \cdot \mathbf{R}_i\|, \quad (8)$$

where N is the total number of nodes, \mathbf{r}_i is the computed position of node i and \mathbf{r}_i^{CBR} is the position of node i predicted by the CBR. We remark that different measures are available, in particular in the stress domain. We limit our analysis to the strain domain because it yields a natural estimate of this deviation and does not rely on a cumbersome definition of the discrete stress tensor.

IV. RESULTS

A. Centre-based models: Models 1, 2 and 3

In this section, we focus on centre-based Models 1, 2 and 3 (See Table I) and study the validity of the CBR for three sizes of tissue, 10×10 , 15×15 and 20×20 cells.

1. Honeycomb

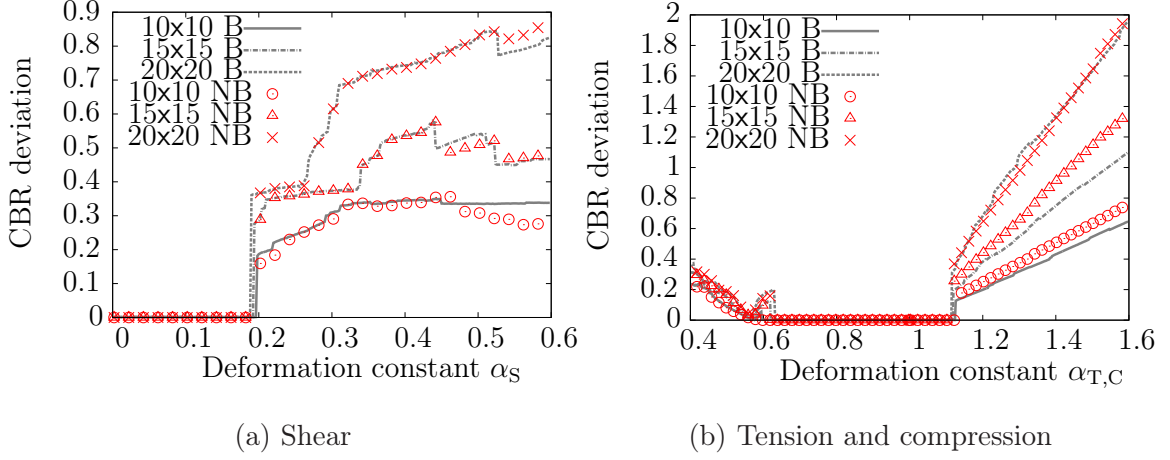


Figure 4. (Color online) Series of plots showing how Model 1 (centre-based, tessellation-based) deviates from the CBR as the deformation parameter, α , varies for (a) shear and (b) tension/compression deformations. For each plot, three sizes of tissues are presented (10x10, 15x15 and 20x20 cells) for “Brownian” (B) and “Non-Brownian” (NB) cases. Results were obtained by computing Eq (8) in the central region for displacements prescribed on the boundary nodes using Eqs (5), (6) and (7). These plots show that: (1) the CBR is only valid in the limit of small deformations; (2) the size of the domain of validity is independent of the size of the tissue; and (3) domains of validity are robust to perturbations.

Here, nodes are arranged on a honeycomb lattice, similar to the one shown in Fig 3 for a tessellation-based model. This situation corresponds to a stress-free configuration with constant rest lengths imposed between connected pairs of nodes throughout the population.

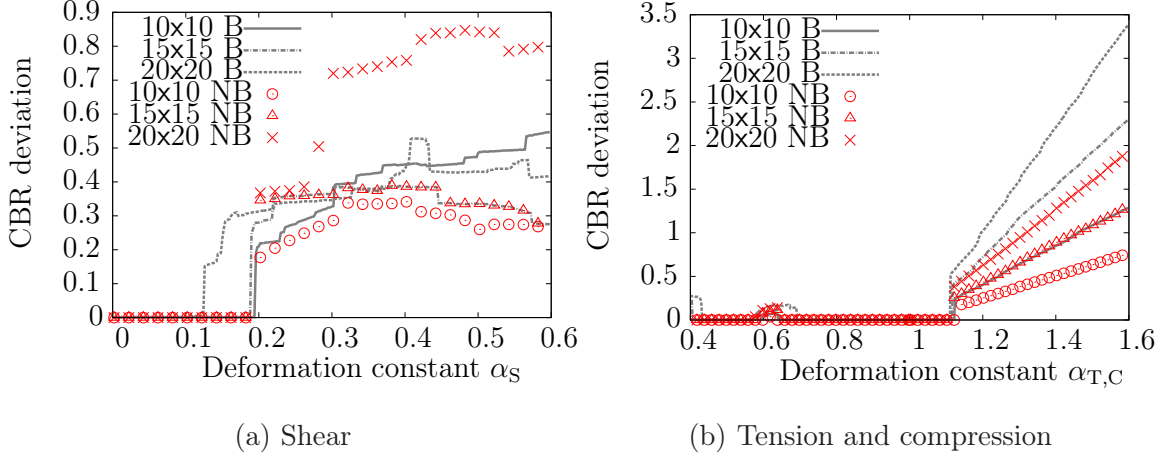


Figure 5. (Color online) Series of plots showing how Model 2 (centre-based, sphere-based) deviates from the CBR as the deformation parameter, α , varies for (a) shear and (b) tension/compression deformations. For each plot, three sizes of tissues are presented (10x10, 15x15 and 20x20 cells) for “Brownian” (B) and “Non-Brownian” (NB) cases. Results were obtained by computing Eq (8) in the central region for displacements prescribed on the boundary nodes using Eqs (5), (6) and (7). These plots show that: (1) the CBR is only valid in the limit of small deformations; (2) domains of validity are independent of the size of the tissue; and (3) domains of validity are robust to small perturbations.

For Model 1, the deviation, Eq (8), is plotted as a function of the deformation parameter, α , for shear in Fig 4a and for compression/tension in Fig 4b. Results are presented for different sizes of tissue and with (B) or without random motion (NB). Equivalent plots for Model 2 are presented in Figs 5a and 5b. These results show that both models exhibit qualitatively similar behaviours. We remark that the domain of validity of the CBR is limited to the small deformations regime, i.e., relatively small values of α . This result is compatible with theoretical analyses obtained for simpler harmonic spring networks, see [14]. We note also that the size of the tissue does not significantly affect the domain of validity of the CBR, although it modifies the amplitude of the average deviation in the large deformation regime, when the CBR fails to describe node locations accurately. This was also observed in [1] and is compatible with the idea that, by prescribing the displacement of boundary nodes, we implicitly impose a homogeneous deformation gradient similar to the representation in Fig 1. Finally, we observe that positions corresponding to the net energy minimizer exhibit very little dependence on “Brownian” perturbations. Bifurcation of results

for “Brownian” tension experiments occurs primarily in the large deformation regime where the CBR fails. This shows stability to small perturbations in domains of CBR validity.

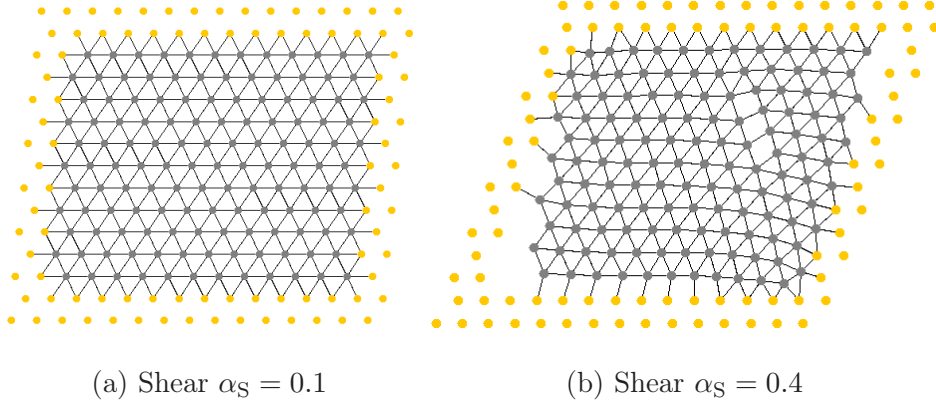


Figure 6. (Color online) Sequence of events corresponding to a shear deformation applied to a “Non-Brownian” cell population (15x15 cells) described using Model 1 for (a) $\alpha_S = 0.1$ and (b) $\alpha_S = 0.4$. The CBR is valid in the limit of small deformations and fails if α_S exceeds a critical value (here $\alpha_S \sim 0.2$) at which stresses in the narrowed corners become large enough.

To understand further why the CBR fails in the large deformation limit, node positions for the tests described above are illustrated for shear experiments, in Fig 6 for Model 1 and in Fig 7 for Model 2. In both cases, the tissue deforms homogeneously, Figs 6a and 7a, until α reaches a critical value at which the stress induced in the narrowed portion of the tissue becomes sufficiently large to create local dislocations, Figs 6b and 7b. The dislocations induce a rearrangement of the nodes and their connectivity, leading to failure of the CBR. As α is increased through this critical value, the deviation from the CBR grows approximately linearly, as the size of the dislocations grows.

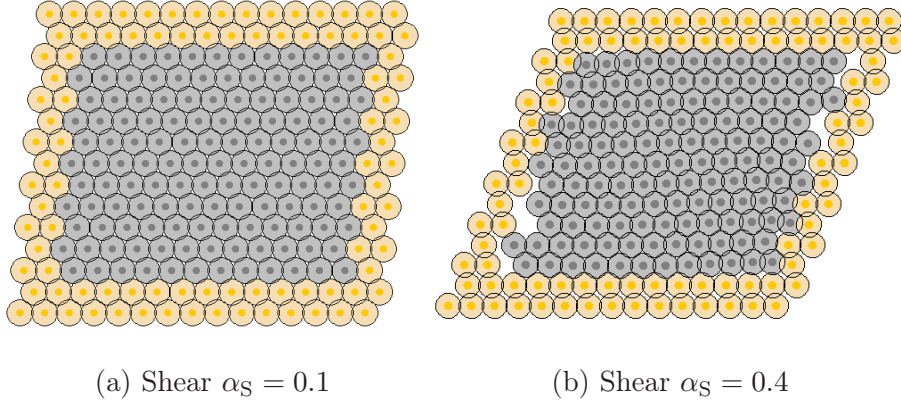


Figure 7. (Color online) Sequence of events corresponding to a shear deformation applied to a “Non-Brownian” cell population (15x15 cells) modelled using Model 2 with (a) $\alpha_S = 0.1$ and (b) $\alpha_S = 0.4$. The CBR is valid in the limit of small deformations and fails if α_S exceeds a critical value (here $\alpha_S \sim 0.2$) at which stresses in the narrowed corners regions become large enough.

The spatial organization of nodes for the tension and compression experiments for Model 1 are presented in Fig 8. In the compressive regime, we observe that, when α_S reaches a critical value, cellular-connectivity is altered. Cells positioned in a given layer are influenced by cells up to two layers away because of how model is set up, i.e., if cells from distant layers get close enough a new spring connection will link them. This is visible in the Delaunay triangulation representation Fig 8a, where the initial connectivity is altered and some (grey) central nodes interact with the second layer of (yellow) boundary nodes. This reorganization destabilizes the homogeneous configuration, causing the CBR to fail. Under tension, the tissue is stretched homogeneously until the vertical connections between internal and boundary cells reach their cut-off length. Incrementing α further causes the distance between the nodes to exceed the cut-off length, generating dislocations, see Fig 8b. Thereafter, the deviation from the CBR increases approximately linearly with $\alpha_{T,C}$, as the size of the dislocations grows. We remark that the slope of this linear dependence is weakly dependent on the “Brownian” perturbation. Indeed, small perturbations dominate tissue behaviour at the onset of plasticity when even the slightest changes in node positions can lead to the appearance of dislocations and the loss of tissue symmetry (compare Fig 8c and 8d).

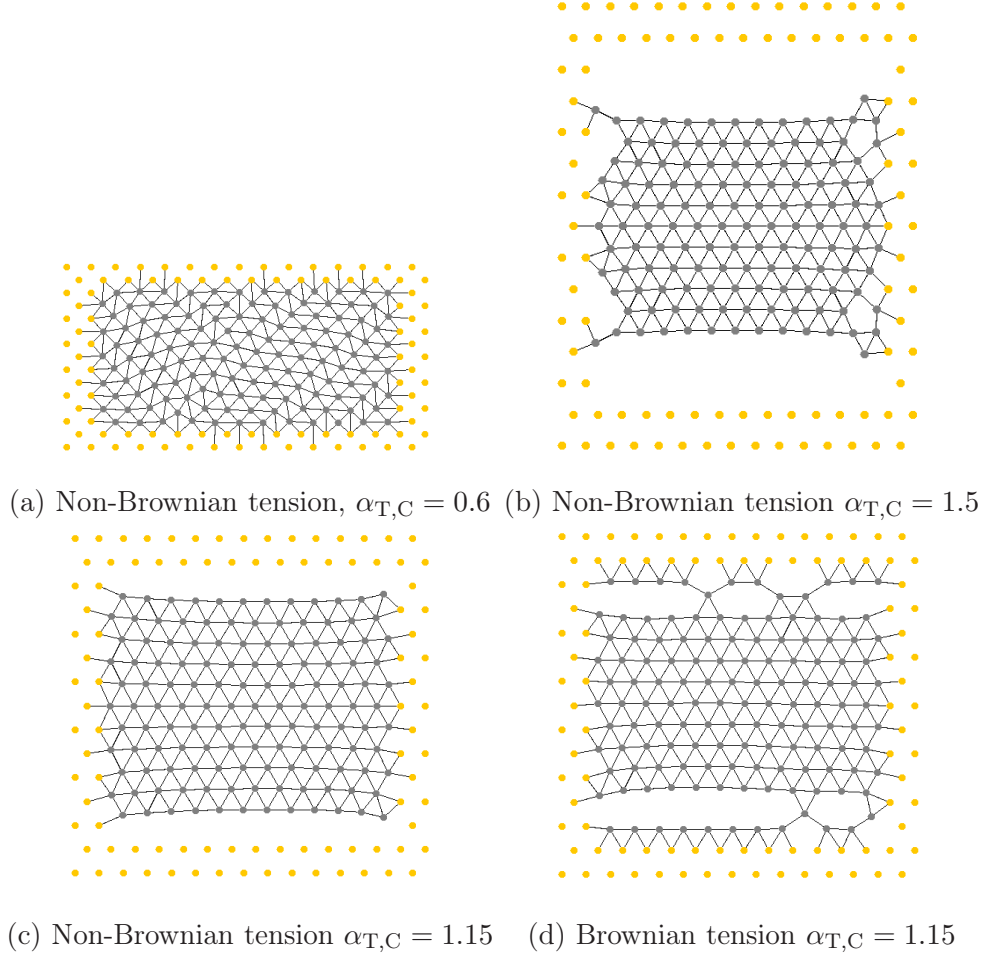


Figure 8. (Color online) Sequence of events corresponding to compression/tension deformations of “Brownian” and “Non-Brownian” cell populations (15x15 cells) described by Model 1 with: (a) $\alpha_{T,C} = 0.6$ “Non-Brownian”; (b) $\alpha_{T,C} = 1.5$ “Non-Brownian”; (c) $\alpha_{T,C} = 1.15$ “Non-Brownian”; and (d) $\alpha_{T,C} = 1.15$ “Brownian”. The CBR is valid in the limit of small deformations and fails if $\alpha_{T,C}$ exceeds a critical value at which either cell connectivities are modified or dislocations appear.

Fig 9 reveals that a similar situation occurs for Model 2. Under tension, the qualitative behaviour replicates that seen for Model 1. Fig 9a shows the position of the nodes after the appearance of the dislocation while Fig 9b shows how symmetry-breaking is induced by “Brownian” perturbations. The main difference between Models 1 and 2 is assessed within their response to compressive loading. Fig 9c shows that the CBR fails for Model 2 when $\alpha_{T,C} \approx 0.6$, but that further compression takes the average deviation back to zero (see Fig 9d). This behaviour is due to the implementation of the sphere-based models. In our model, the radius of interaction of each cell is fixed initially and does not depend on loading.

Therefore, under sufficient compression, interactions are not limited to closest neighbours. In this limit, internal nodes will also interact with both layers of boundary nodes and these additional forces will force homogeneity of cell displacements. Although this model is physically unrealistic, it results from simplifications made in many sphere-based models and is representative of their mechanical behaviour under large compressive loading.

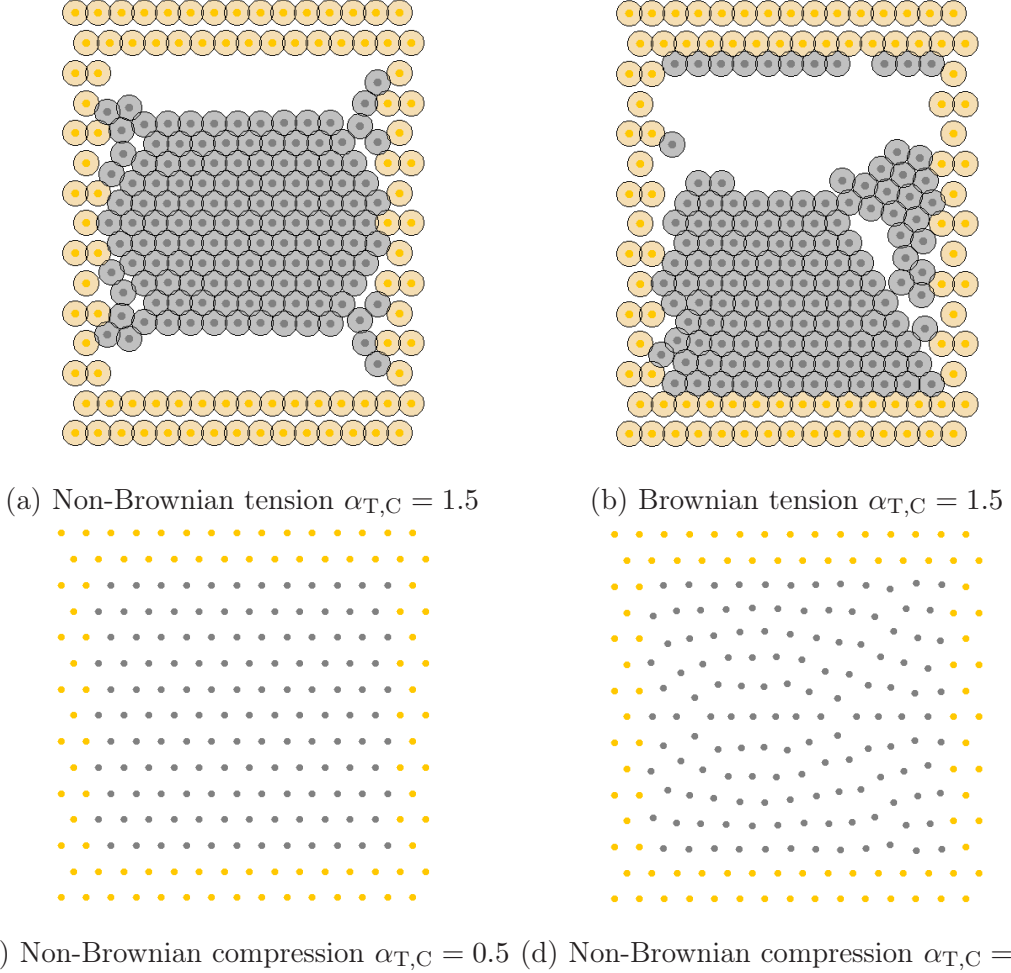


Figure 9. (Color online) Sequence of events corresponding to compression/tension deformations applied to “Brownian” and “Non-Brownian” cell populations (15x15 cells) described via Model 2 with: (a) $\alpha_{T,C} = 1.5$ “Non-Brownian”; (b) $\alpha_{T,C} = 1.5$ “Brownian”; (c) $\alpha_{T,C} = 0.5$; “Non-Brownian” (rescaled for visualization); and (d) $\alpha_{T,C} = 0.62$ “Non-Brownian” (rescaled for visualization). The CBR is valid in the limit of small deformations and fails if α exceeds a critical value for which either cell connectivities are modified or dislocations appear. Figures (c) and (d) illustrate the peculiar behaviour of sphere-based models with constant radii of influence for which the CBR fails for a finite range of values of α before becoming valid again in the limit of large compression.

To explore further this effect of radius, we studied the response of the model for a smaller value of the cut-off length which is equal to the rest length. Results are plotted in Fig 10a for “Non-Brownian” tests. We remark that, in this case, the CBR is not valid under tension because we have eliminated attractive forces. In addition, it seems that the behaviour described above persists only for the smallest tissues (10x10 and 15x15 cells) and is not observed for the larger ones (20x20 cells) for which boundary effects are less important. This suggests that the dominant effect is indeed due to the nonlocal interactions between internal and boundary nodes. This was further confirmed by studying the effect of the force using a different nonlinear force, Model 3, with a cut-off length of 1.1. The results presented in Fig 10b are similar to those obtained with the quasi-spring force under compressive loading and show that the QS and NL forces, although different, exhibit equivalent behaviour on the tissue scale. This corroborates the fact that the anomalous behaviour is induced by nonlocal interactions with boundary nodes and not by the nonlinear nature of the forces.

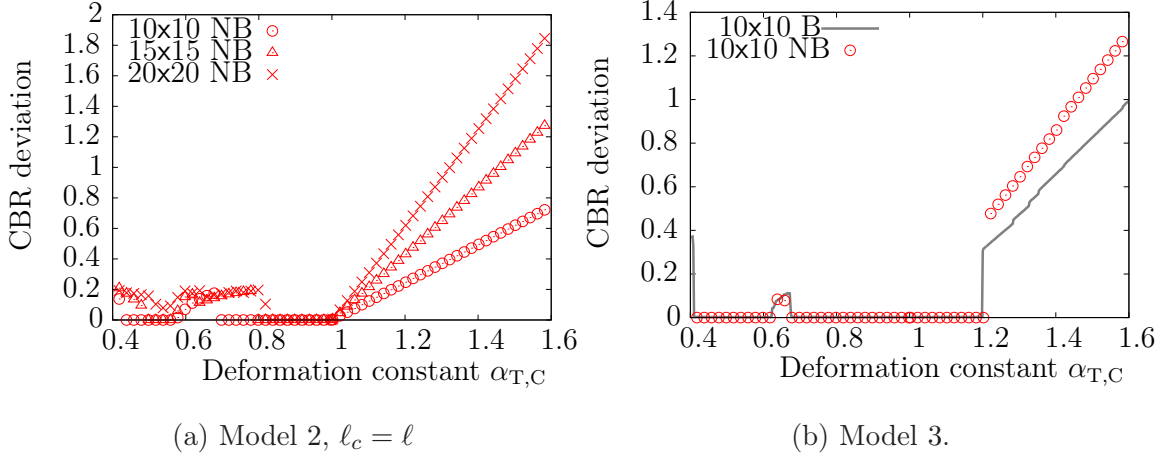


Figure 10. (Color online) Series of plots showing how (a) Model 2 (centre-based, sphere-based) with $\ell_c = \ell = 10 \mu m$ and (b) Model 3 deviate from the CBR as the deformation parameter, α , varies under tension/compression. For (a), three sizes of tissues are presented (10x10, 15x15 and 20x20 cells) for the “Non-Brownian” (NB) case. For (b), one size of tissue is presented (10x10 cells) for the “Brownian” (B) and “Non-Brownian” (NB) cases. Results were obtained by computing Eq (8) in the central region for displacements prescribed on the boundary nodes using Eqs (5), (6) and (7). These plots show that: (1) the peculiar behaviour of sphere-based models with constant radius of interaction disappears with an increase of the size of the tissue or a reduction of the radius of interaction; (2) for $\ell_c = \ell$, the CBR is invalid under tension; and (3) using the NL or QS forces for a sphere-based population does not modify the qualitative deviation from the CBR.

2. Disordered reference structures

In the previous section, the honeycomb (stress-free) reference configuration was obtained by using constant values of the rest lengths for intercellular forces. To investigate the effect of disorder in the reference state on the validity of the CBR, we consider a case for which the rest lengths are chosen from a normal distribution. We fix the mean of this Gaussian distribution to be $\ell = 10 \mu m$ and study the effect of the standard deviation upon the average deviation from the CBR. To generate the physical tissue, we placed cells on a honeycomb lattice and allowed the whole tissue to relax towards a stable equilibrium before applying any deformation. For each value of the standard deviation ($\sigma/\ell = 0.03$, $\sigma/\ell = 0.06$ and $\sigma/\ell = 0.09$), three replicate experiments were performed to account for the stochasticity of the simulations. Results are presented in Figs 11 and 12 for Models 1 and 2 respectively.

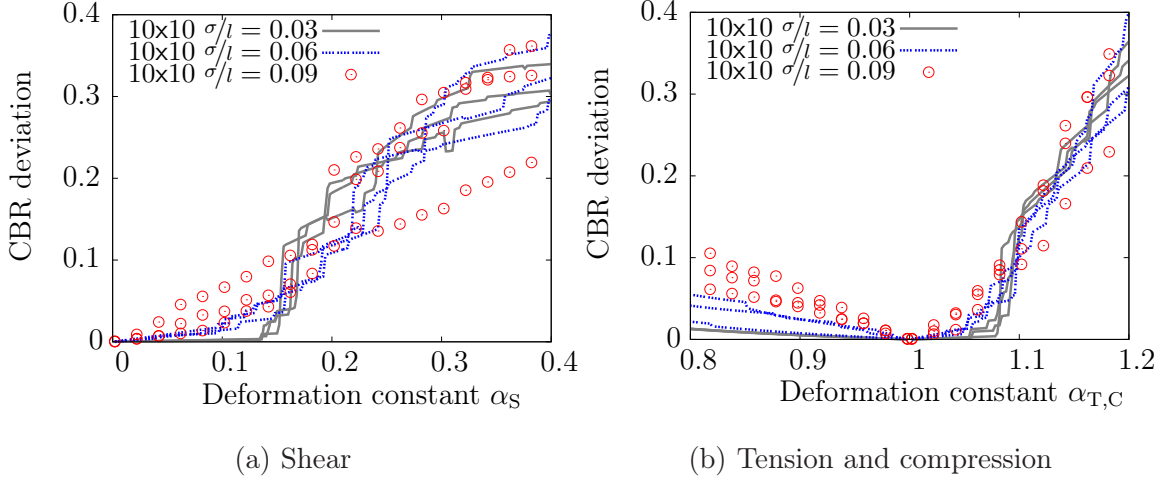


Figure 11. (Color online) Series of plots showing how Model 1 (centre-based, tessellation-based) deviates from the CBR as the deformation parameter, α , varies for (a) shear and (b) tension/compression. Three values of the standard deviation ($\sigma/\ell = 0.03, 0.06$ and 0.09) were used for the “Non-Brownian” case and one size of tissue (10×10 cells). For each value of standard deviation, three replicates are plotted. Results were obtained by computing Eq (8) in the central region for displacements prescribed on the boundary nodes using Eqs (5), (6) and (7). These plots show that: (1) the CBR may not be valid when the reference configuration is an irregular lattice; and (2) for the lowest value of the standard deviation, $\sigma/\ell = 0.03$, the CBR may still provide a good approximation to the displacement field.

In both cases, our results show that the CBR is not exactly satisfied, even in the limit of small deformations. To understand why this happens, it is important to realize that the energy functional characterizing the mechanics of the cell population is sensitive to modifications in the standard deviation. In particular, although cells are initially in stable equilibrium, the number of nodes in the reference state that are close to bifurcation from local energy minima and the amount of prestress increases with σ . The system is, in some sense, in a metastable configuration. *Under such conditions, even the slightest displacement of the boundary nodes may trigger rearrangement on cellular lengthscales (e.g. node permutations) and lead to failure of the CBR.* These cellular-scale phenomena cannot be captured by solid-continuum models, even with higher order or nonlocal theories. *In this sense, the CBR provides a reliable measure of solid-like elastic behaviour.*

Conversely, we see that for relatively small values of the standard deviation, particularly when $\sigma/\ell = 0.03$, the CBR may provide a good representation of node displacements. We

may thus extend the validity of the CBR, with a notion of quasi-validity *in the limit of small deformations and low levels disorder*. In such cases, elastic models derived using the CBR may adequately describe tissue mechanics. We remark that the concept of quasi-validity would be difficult to determine using an analytical approach and that numerical simulations of cellular-scale models are, in this case, helpful in understanding model behaviour.

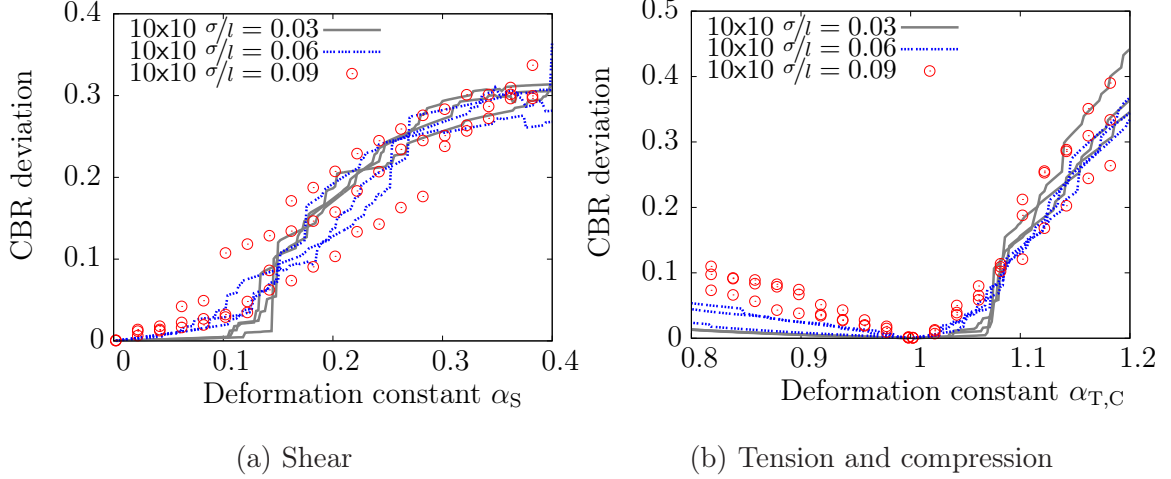


Figure 12. (Color online) Series of plots showing how Model 2 (centre-based, sphere-based) deviates from the CBR as the deformation parameter, α , varies for (a) shear and (b) tension/compression. Three values of the standard deviation ($\sigma/\ell = 0.03, 0.06$ and 0.09) were used for the “Non-Brownian” case and one size of tissue (10×10 cells). For each value of standard deviation, three replicates are plotted. Results were obtained by computing Eq (8) in the central region for displacements prescribed on the boundary nodes using Eqs (5), (6) and (7). These plots show that: (1) the CBR is not valid when the reference configuration does not follow a regular lattice; and (2) for the lowest value of the standard deviation, $\sigma/\ell = 0.03$, the CBR may still represent a good approximation of the displacement field.

B. Vertex-based model: Model 4

We now apply the same techniques to investigate the validity of the CBR for tissue models that use a vertex-based representation. For Model 4, the deviation, Eq (8), is plotted as a function of the deformation parameter, α , for shear in Fig 13a and for compression/tension in Fig 13b. Results are presented for a tissue of size 10×10 both with (B) and without random motion (NB).

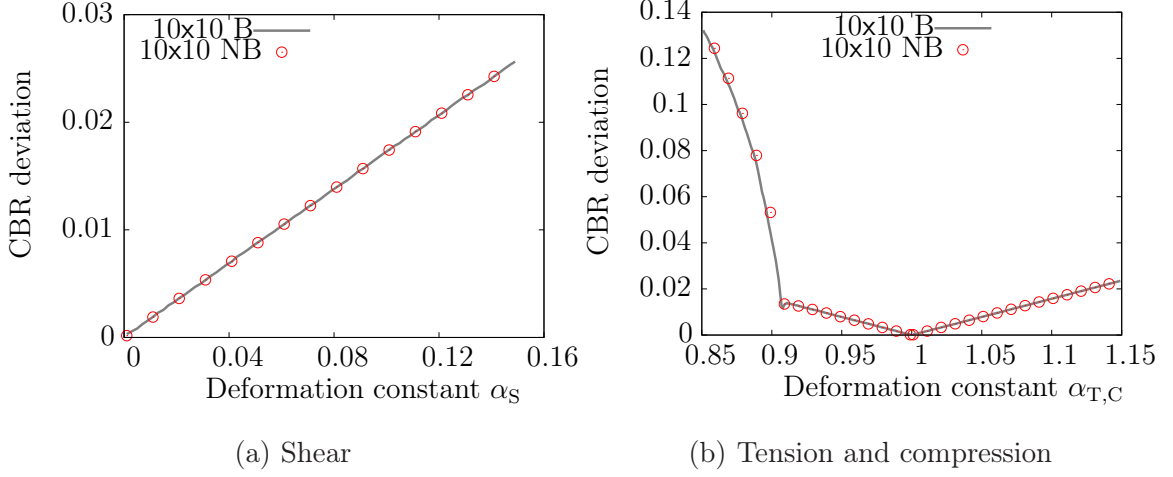


Figure 13. (Color online) Plots of the deviation from the CBR for Model 4 (vertex-based, fixed-connectivity) as a function of the deformation parameter, α , for (a) shear and (b) tension/compression experiments. For each plot, a tissue of size 10x10 cells was used for the “Brownian” (B) and “Non-Brownian” (NB) cases. Results were obtained by computing Eq (8) in the central region for displacements prescribed on the boundary nodes using Eqs (5), (6) and (7). They show that: (1) the CBR is not valid for vertex-based models even when the reference configuration follows a honeycomb lattice; and (2) there are two distinct regions, under compressive loading, of slow linear and fast nonlinear growth of the average deviation.

The results presented in Fig 13 reveal that the behaviour of the vertex-based model is markedly different from that of the other models. In particular, Fig 13 shows that the CBR is never satisfied, even approximately. In the limit of small deformations, the average deviation increases linearly with the deformation constant, starting from zero in the reference configuration. This is evident both under shear, Fig 13a, and under tension/compression, Fig 13b. The cause of this linear deviation is apparent from the spatial distribution of the nodes (see Fig 14): the internal nodes slowly drift away from boundary nodes as they resist shape modification. To understand this phenomenon, recall that positions of vertices are determined through by minimizing deformation (surface area of the cells) and interaction (boundaries of the cells) energies. While cell size in the internal region is constrained by the number of cells and the overall area of the region, cell edges/vertices are positioned via minimization of the interaction energy, a procedure that favours more “circular” shapes. This is also compatible with the idea that vertex-based models can be used for complex viscoelastoplastic rheology of foams (see e.g. Raufaste *et al.* [31]). Interestingly, even

though the CBR does not hold in this situation, the linearity of the deviation for small values of α and the spatial homogeneity of the cells behaviours suggests that a continuum model might still provide a good representation of the tissues mechanics as a whole. These results show that the CBR is not a necessary condition for continuum-like behaviour, but rather a measure of elastic, solid-like behaviour.

We remark further that, under compressive loading, two different regimes can be identified. When the deformation constant is small, the deviation grows linearly with increasing α (see previous discussion), Figs 13b and 14a, until an instability occurs when $\alpha_{T,C} \approx 0.9$ (see Fig 14b). This figure illustrates the inhomogeneous relaxation of vertex positions when α reaches the critical value of instability. We see that the deviation grows linearly until the shape incompatibility between internal and boundary nodes generates a reorganization of intermediate vertices. After this critical value, the deviation is induced by an inhomogeneous drift and becomes nonlinear.

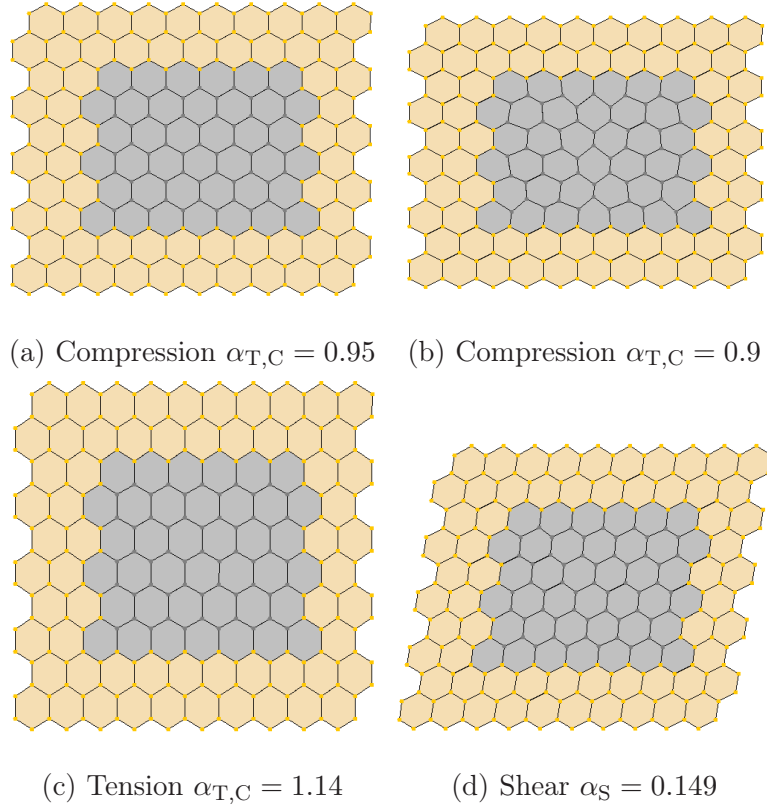


Figure 14. (Color online) Sequence of events corresponding to shear and compression/tension deformations applied to a “Non-Brownian” cell population (10x10 cells) described via Model 4, with: (a) compression, $\alpha_{T,C} = 0.95$; (b) tension, $\alpha_{T,C} = 1.14$; (c) compression, $\alpha_{T,C} = 0.9$; and (d) shear, $\alpha_S = 0.149$. These plots illustrate: (1) the linear growth of the average deviation corresponding to a small drift of the central cells; and (2) the onset of instability corresponding to the nonlinear growth of the average deviation.

V. CONCLUSIONS AND DISCUSSION

In this paper, we have studied the validity of the CBR when applied to different cellular-scale models of biological tissues. We have found that the CBR holds for centre-based models in the limit of small deformations. If the nodes in the reference configuration lie on a stress-free regular lattice then we have shown that the CBR is exactly satisfied for Models 1, 2 and 3. If this is not the case, for example if the rest lengths for intercellular forces are selected from a normal distribution, then the CBR can still provide a good approximation of node positions for low-disorder reference states and a domain of quasi-validity may be defined. If,

however, the disorder is too large, most cells undergo inhomogeneous local rearrangements and a continuum solid description of the system is not possible. In this sense, the CBR provides a measure of continuum solid-like behaviour.

On the other hand, the vertex-based model is based on a different paradigm and does not satisfy the CBR, even for a lattice reference state in the limit of small deformations. In this case, cells are represented via vertices and cellular-connectivity is fixed *ab initio*. For this model, we found that central cells deform more slowly than the boundary cells, leading to linear growth of the deviation from the CBR with increasing α . We also remark that the homogeneous nature of the drift suggests that, even though the CBR fails, a continuum behaviour may exist. This suggests that the CBR can be thought as a measure of solid-like behaviour but not a necessary condition for continuum behaviour. Further, this suggests that the CBR will provide a good measure of continuum-like behaviour in cases when deviation from the CBR is due to cellular-scale perturbations (i.e., Fig 14c) but not when it is due to a homogeneous deviation of the whole tissue (i.e., Fig 14d).

These results open novel perspectives in terms of hybrid and concurrent modelling of biological tissues. Indeed, approaches similar to that proposed in [21] imply that a clear connection exists between the discrete and continuum frameworks. As discussed in the introduction, this connection is typically investigated in 1-D and seldom in 2- or 3-D. Herein, we have shown that, in some situations, this connection can be made via the CBR. This bridge can be used to create a clear and explicit connection between continuum and discrete models, for instance using a discrete virial expression of the stress tensor. Following this idea, hybrid blending over a boundary region could be used in a biological context. For instance, one could imagine developing adaptive models that automatically switch between discrete and continuum descriptions on the basis of limit strain or stress criteria. Further, other AtC methods could be adapted to tissue mechanics, such as adaptive quasicontinuum, bridge scale or peridynamics methods. When compared with hybrid models, an advantage of such one-domain formulations is that cumbersome boundary conditions are not needed. The drawback, however, is that discretization of nonlocal formulations typically gives rise to dense matrices that are more difficult to invert than the sparse matrices produced by discretizing local models.

In addition, we have also demonstrated that the tissue-scale behaviour of cellular-scale models involves a complex nonlinear interplay between the model type (centre-based, vertex-

based), the cell-connectivity, the forces, the set of parameters chosen and even the nature of the deformation. For instance, if the cut-off length between nodes is set to be equal to the rest length, then attractive forces are completely eliminated and the CBR fails to describe node positions in the tension regime. Paradoxically, we have also shown that very different constitutive laws for forces may behave similarly when compared via domains of validity of the CBR. Because of this complexity and nonlinearity, reliable classifications of cellular-scale models do not yet exist and are generally difficult to establish. Such classifications are desirable because of the increasing number of cellular-scale models in the literature and the difficulty to predict their behaviour. Interestingly, Murray *et al.* [25] proposed the classification of 1-D forces via their behaviour in the continuum limit by comparing nonlinear diffusion coefficients for cell density. This approach provides remarkable insight into the dynamics of tissue mechanics but it is unclear how to generalise these 1-D results to higher-dimensional systems. Therefore, here, we suggest that this classification could be done by studying numerically the behaviour of representative portions of tissue undergoing mechanical loading. In particular, we propose that the CBR could be used as a mechanical classification method for cellular-scale models, i.e., *to test if models exhibit a macroscale solid-like behaviour*. A simple example of one such classification could be: (A) models that conform with the CBR in the small deformation limit; (B) models that approximately conform with the CBR in the small deformation limit; (C) models that do not conform with the CBR at all. With this idea, the classification method is adaptive and context dependent. For instance, Model 2 with a cut-off length equal to the rest length is a member (C) for tension deformation, while being a member of class (A) or (B) under compressive loading.

Future work will focus on: (1) comparison with experimental data on tissue deformation; (2) developing a complete classification method for cellular-scale models mechanics; (3) exploring the influence of the reference state upon the macroscale mechanical properties of the tissue in more details (in particular, the impact of prestress); (4) adapting the CBR to account for homogeneous cellular growth; (5) implementing hybrid concurrent models of biological tissues; and (6) adapting other AtC strategies to the biological context.

This work has, for the first time, attempted to develop accurate continuous representations of cellular-scale models of biological tissues in more than one spatial dimension. Moreover, this approximation has allowed the comparison of different cellular-scale models suggesting categories for such models. We anticipate that this work will eventually allow larger biolog-

ical systems to be simulated more realistically using hybrid, discrete-continuum models.

ACKNOWLEDGMENTS

This publication was based on work supported by Award No KUK-C1-013-04, made by King Abdullah University of Science and Technology (KAUST).

APPENDIX

In this appendix, we detail the intercellular forces that are used throughout this paper, starting with the spring force (S force). On node i , this force may be written as

$$\mathbf{f}_i^S = \sum_j \mathbf{f}_{ij}^S \equiv \begin{cases} \lambda \frac{\mathbf{r}_{ij}}{\|\mathbf{r}_{ij}\|} \delta \ell, & \text{for } \delta \leq \frac{\ell_c}{\ell}, \\ \mathbf{0}, & \text{for } \frac{\ell_c}{\ell} < \delta, \end{cases} \quad (9)$$

where \sum_j is the sum over the neighbouring nodes; $\ell_{ij} > 0$ is the rest length of the spring that connects nodes i and j ; and ℓ is a characteristic lengthscale (which we fix to $10 \mu m$). Unless stated otherwise, we assume that $\ell_{ij} = \ell$ for any pair i, j . δ is the nondimensionalized “overlap” parameter defined by

$$\delta = \frac{1}{\ell} (\|\mathbf{r}_{ij}\| - \ell_{ij}). \quad (10)$$

We will also use a quasi-spring force (QS force) defined by

$$\mathbf{f}_i^{QS} = \sum_j \mathbf{f}_{ij}^{QS} \equiv \begin{cases} \lambda \frac{\mathbf{r}_{ij}}{\|\mathbf{r}_{ij}\|} \ell \ln(1 + \delta), & \text{for } \delta \leq 0, \\ \lambda \frac{\mathbf{r}_{ij}}{\|\mathbf{r}_{ij}\|} \delta \ell \exp(-k\delta), & \text{for } 0 < \delta < \frac{\ell_c}{\ell}, \\ \mathbf{0}, & \text{for } \frac{\ell_c}{\ell} < \delta. \end{cases} \quad (11)$$

In equations (9) and (11), λ is the stiffness parameter, k is an adjustable parameter (representing cell-cell attraction) and ℓ_c is the cut-off length. Here, we fix $k = 0.5 \mu m^{-1}$, $\lambda = 15.0 nN \cdot \mu m^{-1}$, $\ell_c = 1.1\ell = 11 \mu m$ and all distances are expressed in μm . We remark that in the limit $\delta \ll 1$, we have

$$\mathbf{f}_{ij}^{QS} = \mathbf{f}_{ij}^S + \mathcal{O}(\delta^2), \quad (12)$$

which means that QS and S forces are equivalent at leading order in the limit of small overlap. The QS force is used to avoid possible instabilities encountered when using sphere-based models (for details see Pathmanathan *et al.* [29]).

We will also consider a more complex description of cell mechanics using the following nonlinear force (NL force)

$$\mathbf{f}_i^{NL} = \sum_j \mathbf{f}_{ij}^{NL} \equiv \begin{cases} \mathbf{F}_{ij}^A + \mathbf{F}_{ij}^E + \mathbf{F}_{ij}^C, & \text{for } \delta \leq \frac{\ell_c}{\ell}, \\ \mathbf{0}, & \text{for } \frac{\ell_c}{\ell} < \delta. \end{cases} \quad (13)$$

In this expression, \mathbf{F}_{ij}^A is the force component describing adhesive interactions between cells; \mathbf{F}_{ij}^E is a force associated with the elastic properties of the cells; and \mathbf{F}_{ij}^C is associated with compressibility effects. These forces are all conservative, so they can be uniquely defined via energy functionals. In this paper, we will employ the forces used in Buske *et al.* [9] and the reader is referred to this paper for further details.

For vertex-based models, we consider only one type of conservative force that combines surface and volume energies, as described in Honda *et al.* [20], Nagai & Honda [27]. We will refer to this force as the Nagai-Honda force (NH force) which is defined by

$$\mathbf{f}_i^{NH} = \nabla_i U, \quad (14)$$

with

$$U = \sum_{\langle ij \rangle} \sigma_{\alpha\beta} |\mathbf{r}_i - \mathbf{r}_j| + \sum_{\alpha} \kappa (S_{\alpha} - S_{\alpha}^0)^2, \quad (15)$$

where i and j are vertices; α and β are cells; distances are expressed in μm ; $\sigma_{\alpha\beta} = 10 \text{ nN}$ is the boundary energy per unit length between cells α and β ; $\kappa = 100 \text{ nN} \cdot \mu m^{-1}$ is a deformation parameter; S_{α} is the surface area of cell α ; and S_{α}^0 is the equilibrium value of the surface area of cell α . For a more detailed description of these forces, the reader is referred to Fig 1 and Eq (6) in [27].

-
- [1] Aghaei, A., Abdolhosseini Qomi, M.J., Kazemi, M.T., & Khoei, A.R. 2009. Stability and size-dependency of Cauchy-Born hypothesis in three-dimensional applications. *International Journal of Solids and Structures*, **46**(9), 1925–1936.
 - [2] Alarcòn, T., Byrne, H.M., & Maini, P.K. 2004. Towards whole-organ modelling of tumour growth. *Progress in Biophysics and Molecular Biology*, **85**(2-3), 451–472.
 - [3] Alexander, S. 1998. Amorphous solids: their structure, lattice dynamics and elasticity. *Physics Reports*, **296**(2-4), 65 – 236.

- [4] Ambrosi, D., & Pezzuto, S. 2012. Active stress vs. active strain in mechanobiology: constitutive issues. *Journal of Elasticity*, DOI 10.1007/s10659-011-9351-4.
- [5] Badia, S., Parks, M., Bochev, P., Gunzburger, M., & Lehoucq, R. 2008. On Atomistic-to-Continuum Coupling by Blending. *Multiscale Modeling & Simulation*, **7**(1), 381.
- [6] Bodnar, M., & Velasquez, J.J.L. 2006. An integro-differential equation arising as a limit of individual cell-based models. *Journal of Differential Equations*, **222**, 341–380.
- [7] Born, M., & Huang, K. 1954. *Dynamical Theory of Crystal Lattices*. Oxford University Press.
- [8] Broedersz, C.P., Sheinman, M., & MacKintosh, F.C. 2012. Filament-Length-Controlled Elasticity in 3D Fiber Networks. *Physical Review Letters*, **108**, 078102.
- [9] Buske, P., Galle, J., Barker, N., Aust, G., Clevers, H., & Loeffler, M. 2011. A Comprehensive Model of the Spatio-Temporal Stem Cell and Tissue Organisation in the Intestinal Crypt. *PLoS Computational Biology*, **7**(1), e1001045.
- [10] Drasdo, D., & Höhme, S. 2005. A single-cell-based model of tumor growth in vitro: monolayers and spheroids. *Physical Biology*, **2**(3), 133–147.
- [11] Ericksen, J.L. 2008. On the Cauchy-Born Rule. *Mathematics and Mechanics of Solids*, **13**(3-4), 199–220.
- [12] Fish, J., Nuggehally, M.A., Shephard, M.S., Picu, C.R., Badia, S., Parks, M. L., & Gunzburger, M. 2007. Concurrent AtC coupling based on a blend of the continuum stress and the atomistic force. *Computer Methods in Applied Mechanics and Engineering*, **196**(45-48), 4548–4560.
- [13] Fozard, J.A., Byrne, H.M., Jensen, O.E., & King, J.R. 2010. Continuum approximations of individual-based models for epithelial monolayers. *Mathematical Medicine and Biology: A Journal of the IMA*, **27**(1), 39–74. PMID: 19617301.
- [14] Friesecke, G., & Theil, F. 2002. Validity and Failure of the Cauchy-Born Hypothesis in a Two-Dimensional Mass-Spring Lattice. *Journal of Nonlinear Science*, **12**(5), 445–478.
- [15] Galle, J., Loeffler, M., & Drasdo, D. 2005. Modeling the Effect of Deregulated Proliferation and Apoptosis on the Growth Dynamics of Epithelial Cell Populations In Vitro. *Biophysical Journal*, **88**(1), 62–75.
- [16] Gardel, M.L., Kasza, K.E., Brangwynne, C.P., Liu, J., & Weitz, D.A. 2008. *Mechanical Response of Cytoskeletal Networks in Methods in Cell Biology*. Elsevier.
- [17] Gibson, L.J. 2005. Biomechanics of cellular solids. *Journal of Biomechanics*, **38**, 377–399.
- [18] Graner, F., & Glazier, J.A. 1992. Simulation of biological cell sorting using a two-dimensional

- extended Potts model. *Physical Review Letters*, **69**(13), 2013–2016.
- [19] Gumbiner, B.M. 1996. Cell Adhesion: The Molecular Basis of Tissue Architecture and Morphogenesis. *Cell*, **84**, 345–357.
 - [20] Honda, H., Tanemura, M., & Nagai, T. 2004. A three-dimensional vertex dynamics cell model of space-filling polyhedra simulating cell behavior in a cell aggregate. *Journal of Theoretical Biology*, **226**(4), 439–453.
 - [21] Kim, Y., Stolarska, M.A., & Othmer, H.G. 2007. A hybrid model for tumor spheroid growth in vitro I: Theoretical development and early results. *Mathematical Models and Methods in Applied Sciences*, **17**(Supp), 1773.
 - [22] Meineke, F., Potten, C., & Loeffler, L. 2001. Cell migration and organization in the intestinal crypt using a lattice-free model. *Cell Proliferation*, **34**, 253–256.
 - [23] Miller, R.E., & Tadmor, E.B. 2003. The Quasicontinuum Method: Overview, applications and current directions. *Journal of Computer-Aided Materials Design*, **9**, 203–239.
 - [24] Moreira, J., & Deutsch, A. 2002. Cellular automaton models of tumor development: a critical review. *Advances in Complex Systems*, **5**, 247–267.
 - [25] Murray, P.J., Edwards, C.M., Tindall, M.J., & Maini, P.K. 2012. Classifying general nonlinear force laws in cell-based models via the continuum limit. *Physical Review E*, **85**, 021921.
 - [26] Murray, P.J., Edwards, C.M., Tindall, M.J., & Maini, P.K. 2009. From a discrete to a continuum model of cell dynamics in one dimension. *Physical Review E*, **80**(3), 031912.
 - [27] Nagai, T., & Honda, H. 2001. A dynamic cell model for the formation of epithelial tissues. *Philosophical Magazine Part B*, **81**(7), 699–719.
 - [28] Osborne, J.M., Walter, A., Kershaw, S.K., Mirams, G.R., Fletcher, A.G., Pathmanathan, P., Gavaghan, D., Jensen, O.E., Maini, P.K., & Byrne, H.M. 2010. A hybrid approach to multi-scale modelling of cancer. *Philosophical Transactions of the Royal Society A: Mathematical, Physical and Engineering Sciences*, **368**(1930), 5013–5028.
 - [29] Pathmanathan, P., Cooper, J., Fletcher, A., Mirams, G., Murray, P., Osborne, J.M., Pitt-Francis, J., Walter, A., & Chapman, S.J. 2009. A computational study of discrete mechanical tissue models. *Physical Biology*, **6**(3), 036001.
 - [30] Pitt-Francis, J., Pathmanathan, P., Bernabeu, M.O., Bordas, R., Cooper, J., Fletcher, A.G., Mirams, G.R., Murray, P., Osborne, J.M., Walter, A., Chapman, S.J., Garny, A., van Leeuwen, I.M.M., Maini, P.K., Rodriguez, B., Waters, S.L., Whiteley, J.P., Byrne, H.M., & Gavaghan,

- D.J. 2009. Chaste: A test-driven approach to software development for biological modelling. *Computer Physics Communications*, **180**(12), 2452–2471.
- [31] Raufaste, C., Dollet, B., Cox, S., Jiang, Y., & Graner, F. 2007. Yield drag in a two-dimensional foam flow around a circular obstacle: Effect of liquid fraction. *European Physics Journal E*, **23**, 217–228.
- [32] Seleson, P., Parks, M.L., Gunzburger, M., & Lehoucq, R.B. 2009. Peridynamics as an upscaling of molecular dynamics. *Multiscale Modeling and Simulation*, **8**(1), 204–227.
- [33] Shenoy, V.B., Miller, R., Tadmor, E.B., Rodney, D., Phillips, R., & Ortiz, M. 1999. An adaptive finite element approach to atomic-scale mechanics—the quasicontinuum method. *Journal of the Mechanics and Physics of Solids*, **47**(3), 611–642.
- [34] Stakgold, I. 1950. The Cauchy relations in a molecular theory of elasticity. *Quarterly of Applied Mathematics*, **8**, 169–186.
- [35] Stolarska, M.A., Kim, Y., & Othmer, H.G. 2009. Multi-scale models of cell and tissue dynamics. *Philosophical Transactions of the Royal Society A: Mathematical, Physical and Engineering Sciences*, **367**(1902), 3525 –3553.
- [36] Wagner, G.J., & Liu, W.K. 2003. Coupling of atomistic and continuum simulations using a bridging scale decomposition. *Journal of Computational Physics*, **190**(1), 249–274.
- [37] Zhou, M. 2003. A new look at the atomic level virial stress: on continuum-molecular system equivalence. *Proceedings of the Royal Society of London. Series A: Mathematical, Physical and Engineering Sciences*, **459**(2037), 2347 –2392.

RECENT REPORTS

12/29	Colorectal Cancer Through Simulation and Experiment	Kershaw Byrne Gavaghan Osborne
12/30	A theoretical investigation of the effect of proliferation and adhesion on monoclonal conversion in the colonic crypt	Mirams Fletcher Maini Byrne
12/31	Convergent evolution of spiny mollusk shells points to elastic energy minimum	Chirat Moulton Shipman Goriely
12/32	Three-dimensional oblique water-entry problems at small dead-rise angles	Moore Howison Ockendon Oliver
12/33	Second weak order explicit stabilized methods for stiff stochastic differential equations	Abdulle Vilmart Zygalakis
12/34	The sensitivity of Graphene 'Snap-through' to substrate geometry	Wagner Vella
12/35	The physics of frost heave and ice-lens growth	Peppin Style
12/36	Finite Element Simulation of Dynamic Wetting Flows as an Interface Formation Process	Sprittles Shikhmurzaev
12/37	The Dynamics of Liquid Drops and their Interaction with Solids of Varying Wettabilities	Sprittles Shikhmurzaev
12/38	Dispersal and noise: Various modes of synchrony in ecological oscillators	Bressloff Lai
12/39	Boundary conditions for free surface inlet and outlet problems	Taroni Breward Howell Oliver
12/40	A Branch and Bound Algorithm for the Global Optimization of Hessian Lipschitz Continuous Functions	Fowkes Gould Farmer
12/41	The Orthogonal Gradients Method: a Radial Basis Functions Method for Solving Partial Differential Equations on Arbitrary Surfaces	Piret
12/42	Squeeze-Film Flow in the Presence of a Thin Porous Bed, with Application to the Human Knee Joint	Knox Wilson Duffy McKee

12/43	Gravity-driven draining of a thin rivulet with constant width down a slowly varying substrate	Paterson Wilson Duffy
12/44	The 'Sticky Elastica': Delamination blisters beyond small deformations	Wagner Vella
12/45	Stochastic models of intracellular transport	Bressloff Newby
12/46	The effects of noise on binocular rivalry waves: a stochastic neural field model	Webber Bressloff
12/47	An Ensemble Bayesian Filter for State Estimation	Farmer
12/48	Simulation of cell movement through evolving environment: a fictitious domain approach	Séguis Burrage Erban Kay
12/49	The Mathematics of Liquid Crystals: Analysis, Computation and Applications	Majumdar
12/50	Fourier spectral methods for fractional-in-space reaction-diffusion equations	Bueno-Orovio Kay Burrage
12/51	Meniscal tear film fluid dynamics near Marx's line	Zubkov Breward Gaffney

Copies of these, and any other OCCAM reports can be obtained from:

**Oxford Centre for Collaborative Applied Mathematics
Mathematical Institute
24 - 29 St Giles'
Oxford
OX1 3LB
England
www.maths.ox.ac.uk/occam**